MOLECULAR SIMULATION
https://doi.org/10.1080/08927022.2021.1880576

Taylor & Francis
Taylor & Francis Group

In-silico strategies of some selected phytoconstituents from *Melissa officinalis* as SARS CoV-2 main protease and spike protein (COVID-19) inhibitors

D. S. N. B. K. Prasanth [a], Murahari Manikanta [b], Vivek Chandramohan[c], Gangadharappa Bhavya[d], Atmakuri Lakshmana Rao[e], Siva Prasad Panda[a], G. S. N. Koteswara Rao[f], Guntupalli Chakravarthi[a], Nayudu Teja[g], Peddireddy Suguna Rani[h], Gummadi Ashu[g], Chittiprolu Purnadurganjali[e], Puvvala Akhil[e], Gorriputti Vedita Bhavani[e] and Tirumalasetti Jaswitha[e]

[a]Pharmacognosy Research Division, K L College of Pharmacy, Koneru Lakshmaiah Education Foundation, Vaddeswaram, India; [b]Department of Pharmaceutical Chemistry, Faculty of Pharmacy, M.S. Ramaiah University of Applied Sciences, Bangalore, India; [c]Siddaganga Institute of Technology, Department of Biotechnology, Siddaganga Institute of Technology, Tumakuru, India; [d]Department of Biotechnology, M.S. Ramaiah Institute of Technology, Bangalore, India; [e]Department of Pharmaceutical Analysis, V. V. Institute of Pharmaceutical Sciences, Gudlavalleru, India; [f]Pharmaceutics Research Division, K L College of Pharmacy, Koneru Lakshmaiah Education Foundation, Vaddeswaram, India; [g]Department of Pharmaceutics, V. V. Institute of Pharmaceutical Sciences, Gudlavalleru, India; [h]Sri Venkateswara University, Department of Pharmacology, Sri Venkateswara University, Tirupati, India

ABSTRACT

Melissa officinalis (Lamiaceae) was used to treat multiple human afflictions. Literary works demonstrated that it has many biological activities. Today's research aims to recognise *Melissa officinalis* phyto-derived anti-viral compounds against main protease and spike protein of COVID-19, to gain insight into the molecular interactions. In the current study, 12 molecules taken from *Melissa officinalis* were analysed through docking, which is derived from the PubMed database. Docking experiments were conducted with Autodock tool. AdmetSAR and Data warrior servers were eventually used for drug-like prediction. Our research shows that three phytoconstituents from *Melissa officinalis*, namely, Luteolin-7-glucoside-3′-glucuronide, Melitric acid-A and Quadranoside-III have exhibited better binding affinity and stability with the targets of COVID-19 main protease and spike protein. The identified substances can be further extended for *in vitro* and *in vivo* studies to assess their effectiveness against COVID-19.

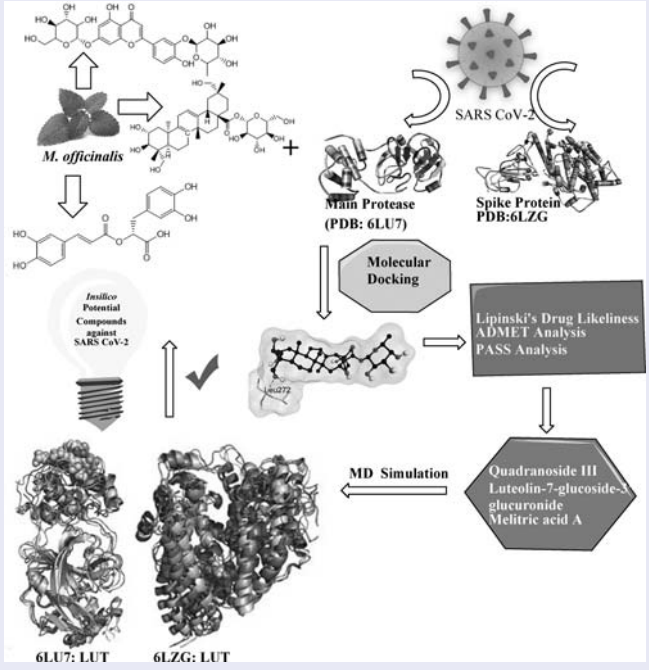

ARTICLE HISTORY
Received 14 September 2020
Accepted 12 January 2021

KEYWORDS
Melissa officinalis; ADMET; Autodock; Physico-chemical; PASS analysis

1. Introduction

WHO has currently stated an emergency condition due to pandemic coronavirus (COVID-19) that has proactively propagating around the entire world. The virus SARS-CoV-2 can easily trigger signs and symptoms such as high temperature, coughing, pneumonia, queasiness, as well as exhaustion

CONTACT D. S. N. B. K. Prasanth dsnbkprasanth@gmail.com

[1,2]. Exact origin of the preliminary transmission to human beings is still unidentified. Presently, there are >100 total genome patterns recognised in the NCBI GenBank, coming from over 10 nations [3]. The variant in between these series is much less than 1%. SARS-CoV-2 has been identified as β-coronavirus which causes severe respiratory tract infection in humans by utilising angiotensin-converting enzyme-2 (ACE2) receptors to infect humans [3]. Chinese experts separated SARS-CoV-2 and also sequenced the genome SARS-CoV-2 on 7 January 2020 [4]. The Main protease (Mpro) is an essential protein required for proteolytic maturation of the virus [5]. Thus, targeting Mpro has the potential to provide effective treatment against SARS-CoV-2 by inhibition of the viral polypeptide cleavage. Spike protein of virus binds to the tissue membrane layer with a receptor-mediated communication which enables a way to host cell. Also makes it possible for the application of well-known protein designed to rapidly develop a version for medicine breakthrough on this brand-new SARS-CoV-2 [6].

The COVID-19 pandemic triggered by SARS CoV-2 has resulted in substantial rates of morbidity and mortality worldwide. The strategy adopted here was to look for *in silico* potential of phyto-constituents against SARS-COV-2 by computational protocols against spike glycoprotein as well as main protease. On the other hand, plants have been essential to human welfare for their uses as therapeutics since ancient times [7,8]. A significant amount of antiviral compounds produced from numerous kinds of plants have been used in many studies [9–11]. Researchers across the globe are screening therapeutic molecules from existing antiviral plant secondary metabolites and are also trying to find novel compounds from medicinal plants to avert this pandemic crisis [12]. *In-silico* based testing has been confirmed to be a handy tool to overcome the obstacles of drug discovery. These computational strategies conserve information in terms of money and time [13–16]. Screening from existing plant metabolites, researchers have been trying to identify and optimise novel compounds from medicinal plants to prevent numerous diseases, including COVID-19.

Thus, we have screened a small library of natural compounds against Mpro and spike protein by *in silico* studies. We have selected *M. officinalis* for the current research, which is an important source of anti-viral agents [17–19]. A traditional Indian medication used hundreds of years to treat different lung diseases, including pneumonia, is the *Melissa officinalis* (Lamiaceae). Several reports have also recently provided convincing and exposing scientific data of its antioxidant, antimicrobial [20] anti-viral [21,22], to treat for moderate Alzheimer [23], neuroprotective [24], anti-cancer [25,26], hepatoprotective [27], anti-depressant [28] and anti-diabetic [29] activities.

The present manuscript therefore attempts to describe in silico potential of *Melissa officinalis* metabolites that have antiviral properties could be aligned as an alternative for COVID-19. The recent emerging viruses, drug targets and drug development methods have thus become very critical challenges in order to identify specific/efficient therapeutics.

2. Materials and methods

2.1. Data source

A list of active phytochemicals was acquired from Indian Medicinal Plants, Phytochemistry and Therapeutic Data Base [30,31].

2.2. Drug-likeliness

Phytochemical components were downloaded from PubChem, and the structures were translated into SDF format and the drug-likeliness of the compounds was evaluated by using Data Warrior program [32].

2.3. Docking studies

2.3.1. Preparation of protein

The protein's atomic coordinates of COVID-19 main protease (PDB ID: 6LU7) and spike protein (PDB ID: 6LZG) were retrieved from the RCSB PDB site [33–35]. The charge assignment, solvation parameters and fragmental volumes to the protein were performed using Autodock Tool 4 (ADT) before study or docking. Protein molecule was further processed for molecular docking [36] (Figure 1).

2.3.2. Ligands preparation and prediction of drug likeliness

The 3D structure of 12 active compounds from *M. officinalis* includes, Quadranoside-III (Pubchem ID: 10327092), Luteolin-7-glucoside-3′-glucuronide (Pubchem ID: 44258136), Melitric acid – A (Pubchem ID: 10459878), Labiatenic acid (Pubchem ID:5281792), Nepetoidin-A (Pubchem ID: 5316820), Salvianic acid-A (Pubchem ID: 11600642), (R)-Citronellal (Pubchem ID:75427), 5-Ketooctanoic acid

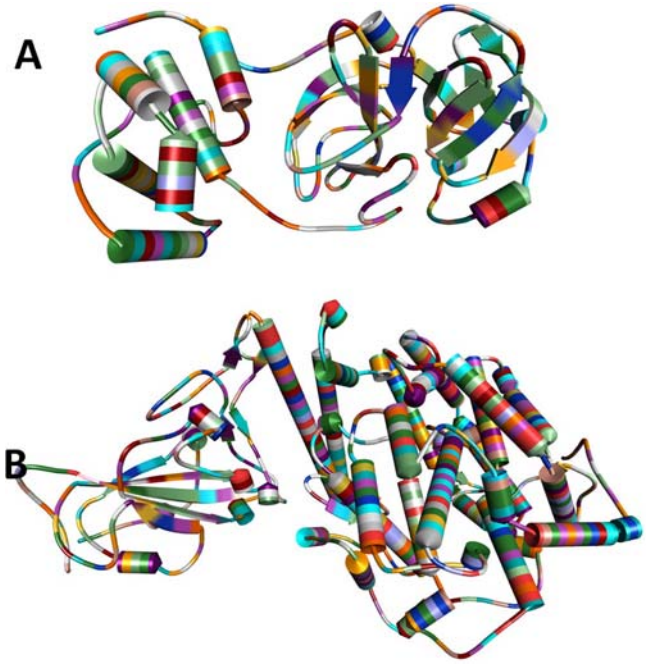

Figure 1. (Colour online) 3D Structures of Proteins (A) Main Protease (PDB ID: 6LU7) and (B) Spike Protein (PDB ID: 6LZG).

(Pubchem ID:128859), Conhydrinone (Pubchem ID:426124), gamma-Coniceine (Pubchem ID:442632) and 5-Ketooctanal (Pubchem ID: 12538121) were retrieved from PubChem database [37]. Drug likeliness properties of ligands were analysed using Data Warrior tools for the selected active compounds [38] (Figure 2).

2.3.3. Active site prediction

An important step is a precise prediction of active sites throughout bioinformatics. During this analysis, Active Site of Main Protease and Spike Protein was projected (Figure 3) by Biovia Drug Discovery Studio Visualizer 2020 (PDB ID: 6LU7, 6LZG).

2.3.4. Validation of complex structures of the protein–ligand

Autodock 4.0 technique has been validated to ensure the simulated screening process using the corresponding co-crystallised ligands of target proteins. Autodock 4.0 reflects a reliable RMSD score with target-receptor binding [34].

2.4. Compound screening using Autodock program

The Autodock wizard was used as docking source to check molecular compound libraries with Autodock software [39]. Ligands were found flexible during the docking process, and protein was kept rigid. Grid parameter configuration file was created for autodock with dimensions of ($X = -10.711837$, $Y = 12.411388$, $Z = 68.831286$ for 6LU7; $X = -31.495980$, $Y = 24.224738$, $Z = -14.498712$ for 6LZG). In this study, amino acids in the active protein site interacting with ligands were identified. Root-mean-square deviation (RMSD) of less than 1.0 Å were deemed optimal and grouped to determine the desirable relation. The best ligand was selected based on the binding affinity at the active pocket with the respective target protein.

2.5. Analysis and visualisation

Biovia Drug Discovery Studio 2020 was used to examine the docking site visually, and the results were confirmed with Autodock Vina [40].

2.6. ADMET analysis

ADMET of the ligands is their pharmacokinetic properties that are required to be examined to establish their function inside the body. The ADMET inheritance of ligands was predicted by making use of admetSAR [41,42].

2.7. PASS computer program

The *Manosa officinalis* prediction for anti-viral behaviour was generated with software support of PASS. PASS is a computer-based system used for estimating various kinds of physiological actions for several phyto-constitutional compounds. The calculated effect of a compound is projected as probable (Pa) activity and possibly (Pi) inactivity. Substances which disclose Pa higher than Pi are the only components deemed possible for a particular medicinal activity [43–45].

2.8. Molecular dynamics simulation

MD simulation was carried out with GROMACS 2019.4 [46] based on the GROMOS96 force field as reported previously [34,47]. All MDs were carried out on a GPU enabled workstation. We carried out MD simulations for the following list of complexes: (i) 6LU7-APO, (ii) 6LU7-LUT, (iii) 6LU7-QUA, (iv) 6LGZ-APO, (v) 6LZG-LUT and (vi) 6LZG-MEL. The primary Molecular dynamics was done using the PDB coordinate file for the proteins PDB ID 6LU7 and PDB ID 6LGZ as the starting point. Residues missing in the 6LU7 and 6LGZ of the PDB structure were added using Discovery studio [48]. The system was arranged in a cubic box (size 1.0 nm), solvated with water (SPC) and further neutralised by addition of sodium ions. For the docked complex MD, the ligand topology file for PDB ID 6LU7 and PDB ID 6LGZ were generated using the PRODRG2 server setup [49] Using the steepest descent algorithm, energy minimisation was done at 1000 steps. Position restraints were employed to 6LU7 and 6LZG, after that a temperature balancing (300 K) and pressure balancing (1 bar) was executed at 50,000 ps each. The MD production runs were then conducted for 50 ns, maintaining temperature at 300 K and pressure at 1 bar. Graphs from the MD simulations data were plotted using Xmgrace [50]. MM-PBSA calculations were performed for last 20 ns of respective complexes.

3. Results

3.1. Drug likeliness properties

Data Warrior software was used to study the physicochemical properties of selected 12 active compounds. Except for three compounds, remaining all the compounds obeyed Lipinski's rule (Table 1). The basic physicochemical properties of TPSA and AMR mainly include drug intake, distribution and penetration functions [51].

3.2. Molecular docking studies

Molecular docking was conducted on 12 phytoconstituents acquired from *M. officinalis* to discover a prospective COVID-19 candidate against main protease and spike protein (PDB ID: 6LU7 and 6LZG). Such 12 compounds were bound to the target enzyme COVID-19 and rated based on their dock results. Top three compounds with a dock value of −8.0 kcal/mol or lower for 6LU7 interactions and −9.0 kcal/mol or lower for 6LZG communications were considered to be a good illustration of COVID-19 control. For a detailed review, refer to Table 2. A total of 3 compounds were chosen based on 6LU7 and 6LZG binding interactions (Figures 4–10).

3.3. Studies on molecular interaction

The rigid docking results were foreseen utilising Discovery Studio for communications assessment. Tables 3 and 4 provided the best binding sites for protein–ligand interaction.

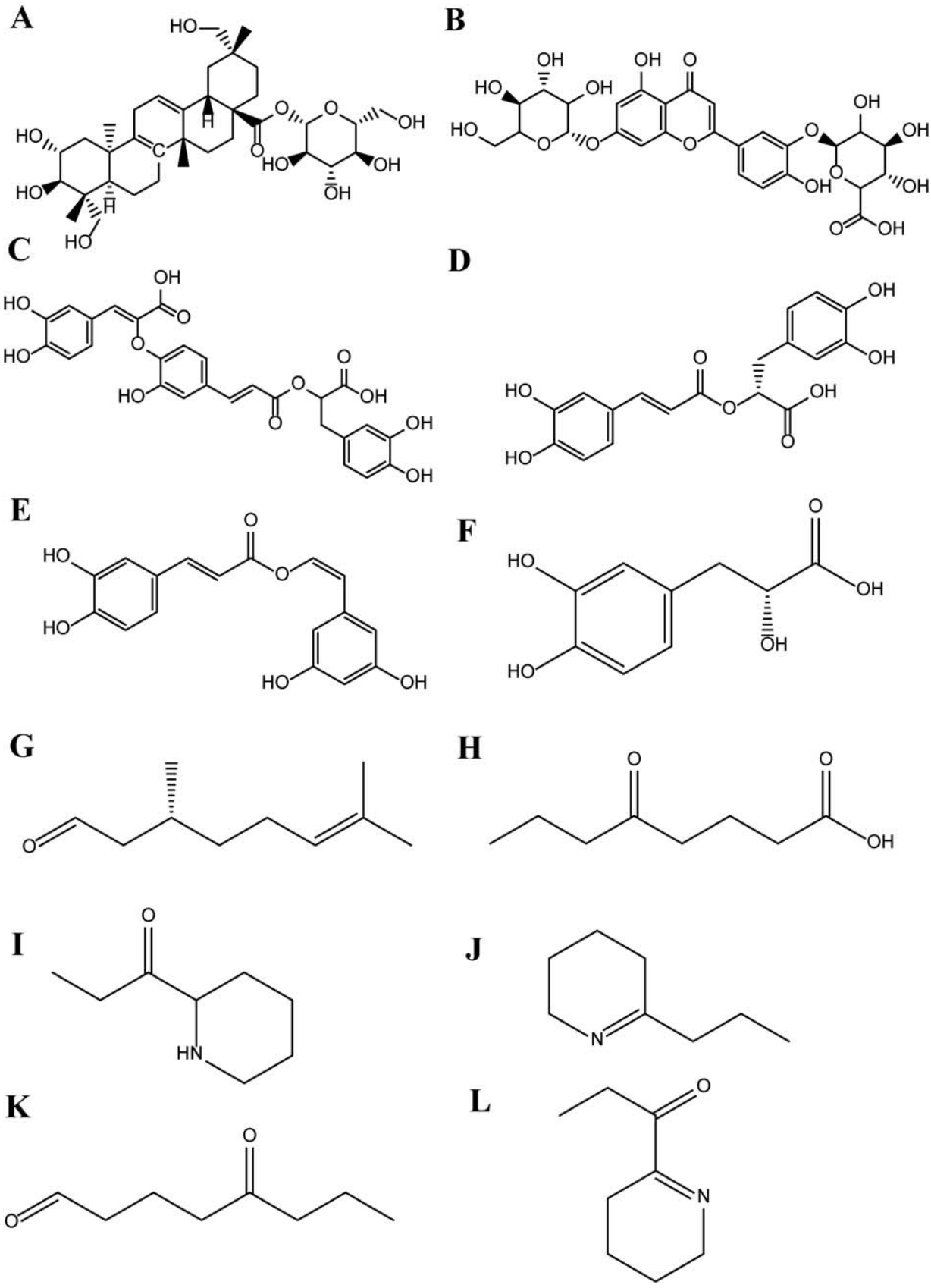

Figure 2. 2D structures of the ligands utilised in the study (A) Quadranoside-III, (B) Luteolin-7-glucoside-3′-glucuronide, (C) Melitric acid – A, (D) Labiatenic acid, (E) Nepetoidin-A, (F) Salvianic acid-A, (G) (R)-Citronellal, (H) 5-Ketooctanoic acid (I) Conhydrinone, (J) Gamma-Coniceine, and (K) 5-Ketooctanal (L) 1′-Oxo-gamma-coniceine.

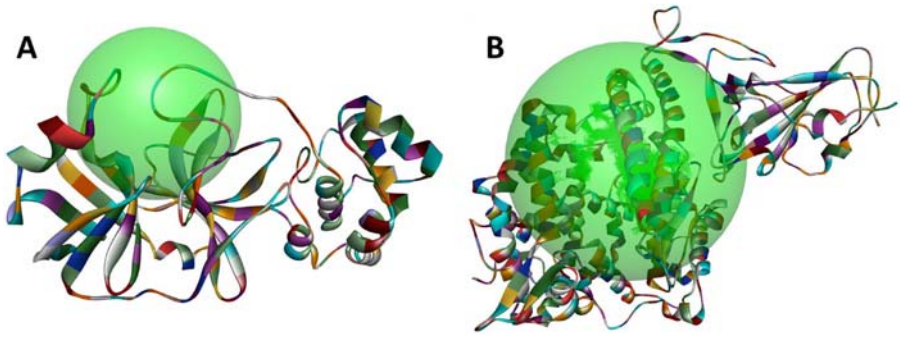

Figure 3. (Colour online) Prediction of Active sites by Drug Discovery Biovia 2020 (A) Main Protease (PDB ID: 6LU7) (B) Spike Protein (PDB ID: 6LZG).

Table 1. Physicochemical properties of active compounds and accordance with the rule of drug-likeliness.

Sr. No.	Ligand	MW	Clogp	HBA	HBD	TPSA	MR	nRB	No. of Deviations
1	Gamma-Coniceine	125.214	2.0281	1	0	117.79	45.47	2	0
2	Labiatenic acid	360.317	1.4502	8	5	263.03	91.40	7	0
3	(R)-Citronellal	154.252	3.1371	1	0	148.31	49.91	5	0
4	Luteolin 7-glucoside-3′-glucuronide	625.51	−3.5387	17	10	407.62	140.24	7	1
5	Nepetoidin A	314.292	2.2497	6	4	239.17	85.14	5	0
6	Melitric acid A	538.46	2.6975	12	7	387.95	136.10	11	1
7	Quadranoside III	666.846	1.5963	11	8	456.88	172.11	5	1
8	Salvianic acid A	198.173	−0.116	5	4	142.67	48.00	3	0
9	1′-Oxo-gamma-coniceine	139.197	0.9751	2	0	121.78	45.67	2	0
10	5-Ketooctanoic acid	158.196	1.3743	3	1	136.41	42.54	6	0
11	5-Ketooctanal	142.197	1.5116	2	0	131.85	40.97	6	0
12	Conhydrinone	141.213	0.925	2	1	122.77	45.37	2	0

The strongest connection was noticed in the Quadranoside III with main protease protein complexes of −8.6 kcal/mol. The main protease with Quadranoside III complex formed three hydrogen bonds, i.e. LYS A:137; 4.60 A°, ASN A:238; 4.52 A °, GLU A:288; 4.82 A° and one hydrophobic interaction with LEU A:272; 4.46 A°. Luteolin-7-glucoside-3′-glucuronide-main protease complex formed three hydrogen bonds i.e. PHE A:219; 5.16 A°, ASN A:221; 3.75, 3.78, 4.67 A°, ASP A:263; 3.50, 3.90 A° and one hydrophobic interaction with LEU A:220; 4.22 A°. Melitric acid A formed three hydrogen bond interactions with GLN A:110; 4.80, 5.23 A°, ASN A:151; 4.23 A°, ILE A:249; 3.34 A° and five hydrophobic interactions with the residues of VAL A:104; 7.12 A°, ILE A:106; 5.62 A°, PHE A:294; 4.40 A°, PRO A:293; 4.44 A°, ILE A:249; 4.77 A°. None of the compounds exhibited electrostatic interactions with the protein.

The best possible associate with Luteolin-7-glucoside-3′-glucuronide (−10.1 kcal/mol) of the phytochemicals was identified to be spike protein (6LZG) of SARS-CoV-2 (Table 4). The spike protein with Luteolin-7-glucoside-3′-glucuronide complex formed seven hydrogen bonds, i.e. TYR A:196; 6.05 A°, GLU A:564; 5.23 A°, LYS A:562; 4.36 A°, GLY A:395; 4.95 A°, ASN A:397; 2.98 A°, ARG A:514; 5.03 A°, GLU A:398; 4.76 A° and two amino acids are involved in the formation of hydrophobic interactions TYR A: 202; 6.27 A°, GLY A:205; 5.85 A°.

Table 2. Molecular docking of selected compounds with Main Protease target protein (PDB ID:6LU7) and Spike Protein (PDB ID: 6LZG).

		Dock Score (kcal/mol)	
Sr. No	Ligands	6LU7	6LZG
1	Luteolin-7-glucoside-3′-glucuronide	−8.5	−10.1
2	Melitric acid A	−8.2	−10
3	Quadranoside III	−8.6	−9.2
4	Labiatenic acid	−7.1	−8.9
5	Nepetoidin A	−7	−7.1
6	Salvianic_acid	−5.9	−7.1
7	(R)-Citronellal	−4.5	−6.3
8	1′-Oxo-gamma-coniceine	−4.6	−6.2
9	Conhydrinone	−4.4	−5.7
10	gamma-Coniceine	−4.6	−5.4
11	5-Ketooctanoic acid	−4.5	−5.2
12	5-Ketooctanal	−3.7	−5.1

3.4. ADME/T evaluation by using admetSAR

The ADMET attributes of ligands have been calculated using admetSAR. All the substances demonstrated good human intestinal absorption (HIA) and penetration of the blood–brain barrier (BBB). None of them were found carcinogenic. None of the substances demonstrated negative for AMES. Table 5 lists the tests of HIA, BBB, LD_{50} for compounds.

3.5. PASS predictions for anti-viral activity

Virtual PASS version collected the biological activity range of previously identified plant constituents. Such projections were flexibly interpreted and given in Table 6.

3.6. Molecular simulation studies of 6LZG

The Root Mean Square Deviation (RMSD) is frequently used to measure the steadiness of an enzyme or drug bounded enzyme during the simulation period [1]. We examined

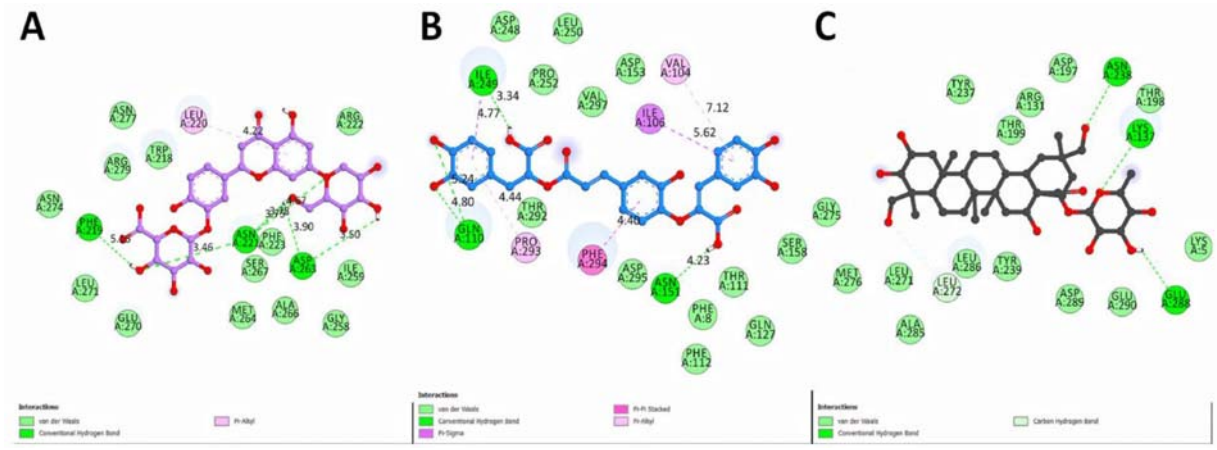

Figure 4. (Colour online) 2D Interactions of ligands with Main protease (6lu7). (A) Quadranoside III (B) Luteolin-7-glucoside-3′-glucuronide (C) Melitric acid A.

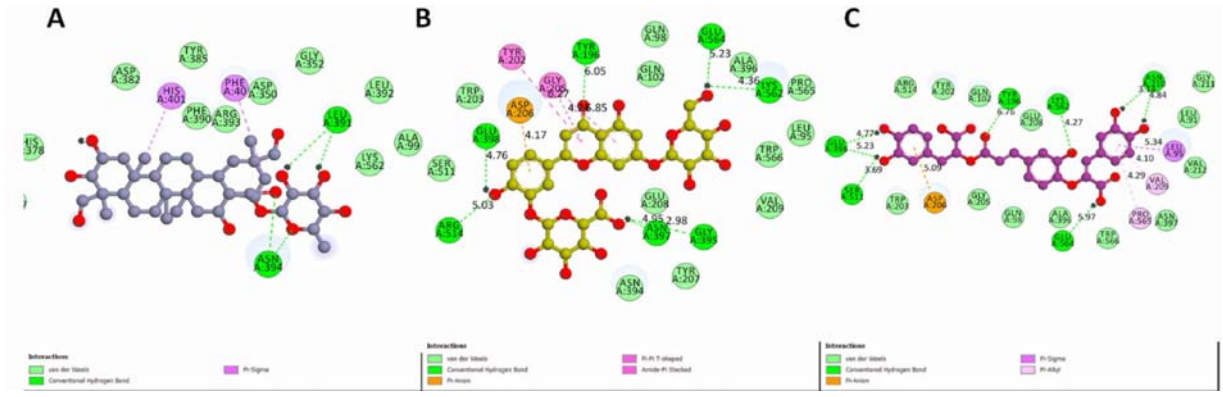

Figure 5. (Colour online) 2D Interactions of ligands with Spike Protein (6lzg). (A) Luteolin-7-glucoside-3′-glucuronide (B) Melitric acid A (C) Quadranoside III.

RMSD of the simulated system over time by measuring the deviation of 6LZG with its crystal structure (APO). Figure 11 (A) shows that the RMSD of systems reaches equilibration state at 50 ns and the analysis was performed within 10–50 ns frames. The 6LZG-LUT and 6LZG-MEL were found to deviate from crystal conformation giving an indication that the bound state of drugs may persuade the structure of protein. Average values of RMSD of the systems 6LZG-APO, 6LZG-LUT and 6LZG-MEL were found to be 0.363, 0.238 and 0.221 nm, respectively, confirming the stability of compounds during the simulation time.

We analysed the root mean square fluctuations (RMSF) of 6LZG-APO, 6LZG-LUT and 6LZG-MEL systems to evaluate the lack of stability area wise. RMSF values for 6LZG-APO, 6LZG-LUT and 6LZG-MEL were shown in Figure 11(B). RMSF plot indicates that residues of alpha helix and beta sheet region are not changing in the 50 ns simulation period. Average values of 6LZG-APO, 6LZG-LUT and 6LZG-MEL were found to be 0.116, 0.118 and 0.128 nm, respectively.

Further, we calculated the radius of gyration (Rg) of protein to understand the influence of compounds on compactness of the protein. Rg values for the protein alone, 6LZG-APO and protein–ligand complexes of 6LZG-LUT and 6LZG-MEL were shown in Figure 11(C). Mean Rg value of 6LZG-APO, 6LZG-LUT and 6LZG-MEL were found to be 2.530, 2.496 and 2.519 nm, respectively. From Figure 11(C) it was clear that observable deviations recorded before 50 ns in all the simulations indicating that ligands strongly bind to the active site and maintained the stability of protein structure.

The binding pattern of protein–ligand complex was analysed for its hydrogen-bonding interactions. Hydrogen-bonding interactions of protein–ligand complexes 6LZG-LUT and 6LZG-MEL were shown in Figure 11(D). The 6LZG-LUT and 6LZG-MEL were found to be 3 and 8, respectively, indicating the strong bonding interactions throughout the 50 ns of MD simulations.

Root Mean Square Deviation (RMSD) is frequently used to measure the steadiness of an enzyme or drug bounded enzyme during the simulation period [1]. We examined the RMSD of the simulated system over time by measuring the deviation of 6LU7 with its crystal structure (APO). Figure 12(A) shows that the RMSD of systems reached the equilibration state at 10 ns and the analysis was performed within 10–50 ns frames. The 6LU7-LUT and 6LU7-QUA were found to deviate from crystal conformation giving an indication that the bound state of drugs may persuade the structure of protein. Average values of RMSD of the systems 6LU7-APO, 6LU7-LUT and 6LU7-QUA were found to be 0.376, 0.275 and 0.345 nm, respectively, confirming the stability of compounds during the simulation time.

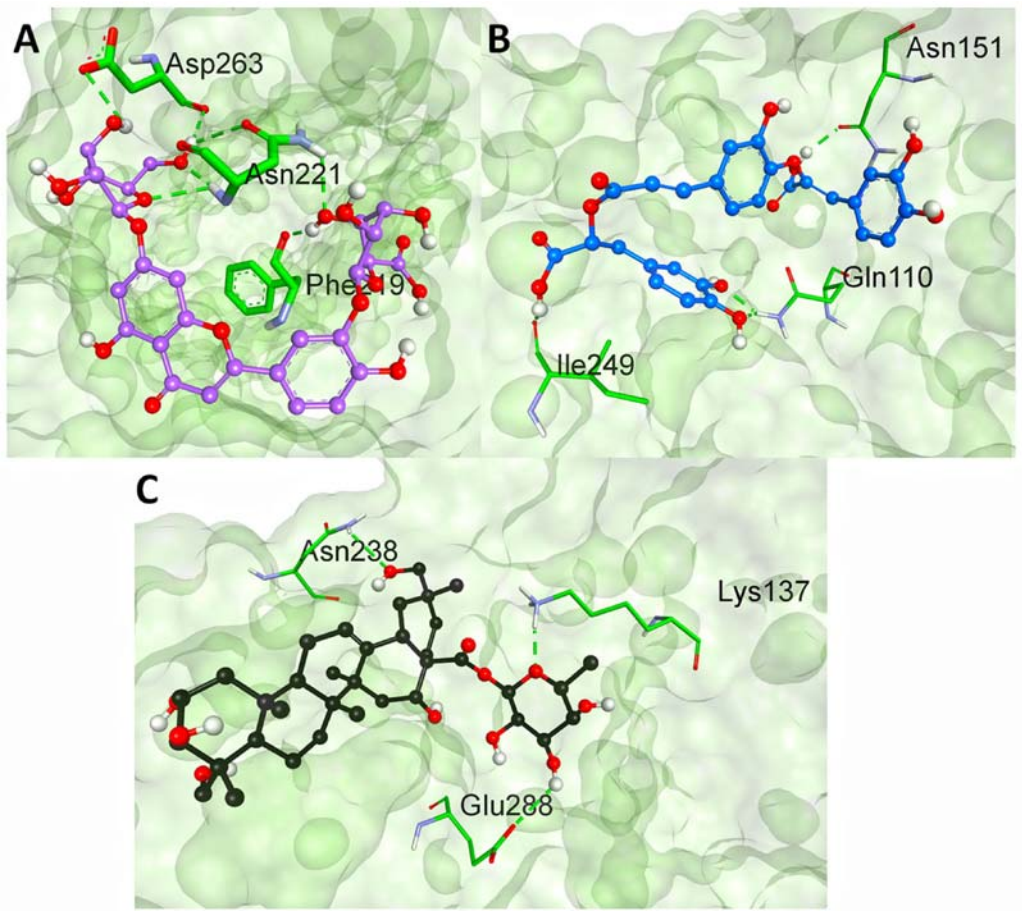

Figure 6. (Colour online) 3D Interactions of ligands with the COVID-19 Main Protease via Hydrogen Bonding. (A) Quadranoside III (B) Luteolin-7-glucoside-3′-glucuronide (C) Melitric acid A.

We analysed the root mean square fluctuations (RMSF) of 6LU7-APO, 6LU7-LUT and 6LU7-QUA systems to evaluate the lack of stability area wise. RMSF values for 6LU7-APO, 6LU7-LUT and 6LU7-QUA were shown in Figure 12(B). RMSF plot indicates that residues of alpha helix and beta sheet region were not changing in the 50 ns simulation period. The average value of 6LU7-APO, 6LU7-LUT and 6LU7-QUA were found to be 0.156, 0.155 and 0.192 nm, respectively.

Further, we calculated the radius of gyration (Rg) of protein to understand the influence of drugs on compactness of the protein. Rg values for the protein alone, 6LU7-APO and protein–ligand complexes of 6LU7-LUT and 6LU7-QUA were shown in Figure 12(C). Mean Rg values of 6LU7-APO, 6LU7-LUT and 6LU7-QUA were found to be 2.243, 2.226 and 2.256 nm, respectively. From Figure 12(C) it was clear that observable deviations recorded before 50 ns in all the simulations indicating that ligands strongly bind to the active site and maintained the stability of protein structure.

The binding pattern of protein–ligand complexes were analysed for their hydrogen-bonding interactions. Hydrogen-bonding interactions of protein–ligand complexes 6LU7-LUT and 6LU7-QUA were shown in Figure 12(D). The 6LU7-LUT and 6LU7-QUA were found to be 2 and 7, respectively, indicating the strong bonding interactions throughout the 50 ns of MD simulations.

3.6.1. MM-PBSA

The binding affinity of 6LU7 with LUT and QUA was examined using relative binding strength at active centre pocket. Binding energy values were provided in Table 7. Binding free energy values of 6LU7 with LUT and QUA were observed to be −84.035 ± 16.402 and −82.056 ± 15.906 kJ/mol indicating that LUT has a strong binding affinity with the 6LU7. Whereas, the binding free energy of 6LZG with LUT and MEL was found to be −106.398 ± 25.384 and −137.222 ± 18.027 kJ/mol indicating MEL with better binding affinity with 6LZG. Further, we calculated the active site residues involved in interaction with the drug molecules for 30–50 ns frame. The interactions of 6LU7 with LUT and QUA and 6LZG with LUT and MEL were tabulated (Table 7).

Further, we calculated the time scale dynamics studies of 6LU7 and 6LZG systems in 0, 100, 200 and 300 ns for 6LU7 systems and 0, 50 and 100 ns for 6LZG systems. The result were depicted in Figure 13.

4. Discussion

Coronaviruses have a long history of human and animal infection involving diseases of the gastrointestinal, urinary, liver and central nervous system [52]. A newly arrived SARS-CoV-2 now poses major threats to human health [53]. Main focus was on clinical management that includes infection

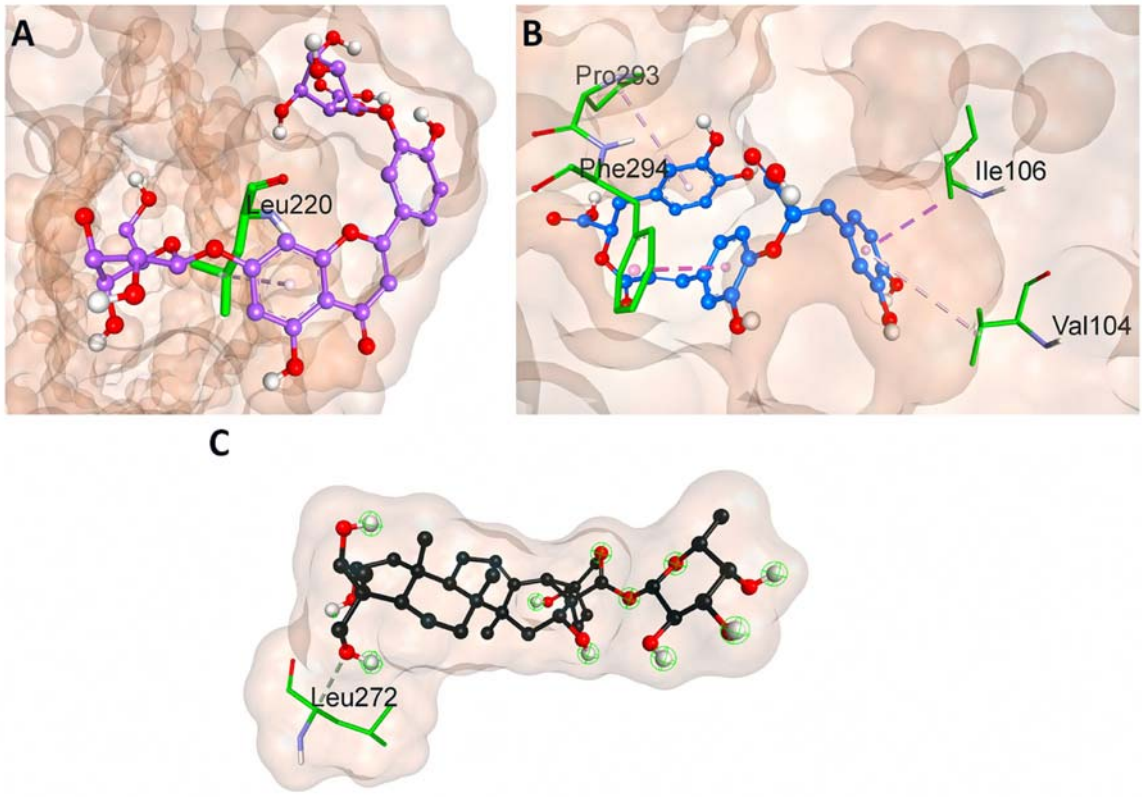

Figure 7. (Colour online) 3D Interactions of ligands with the COVID-19 Main Protease via Hydrophobic bonding. (A) Quadranoside III (B) Luteolin-7-glucoside-3′-glucuronide (C) Melitric acid A.

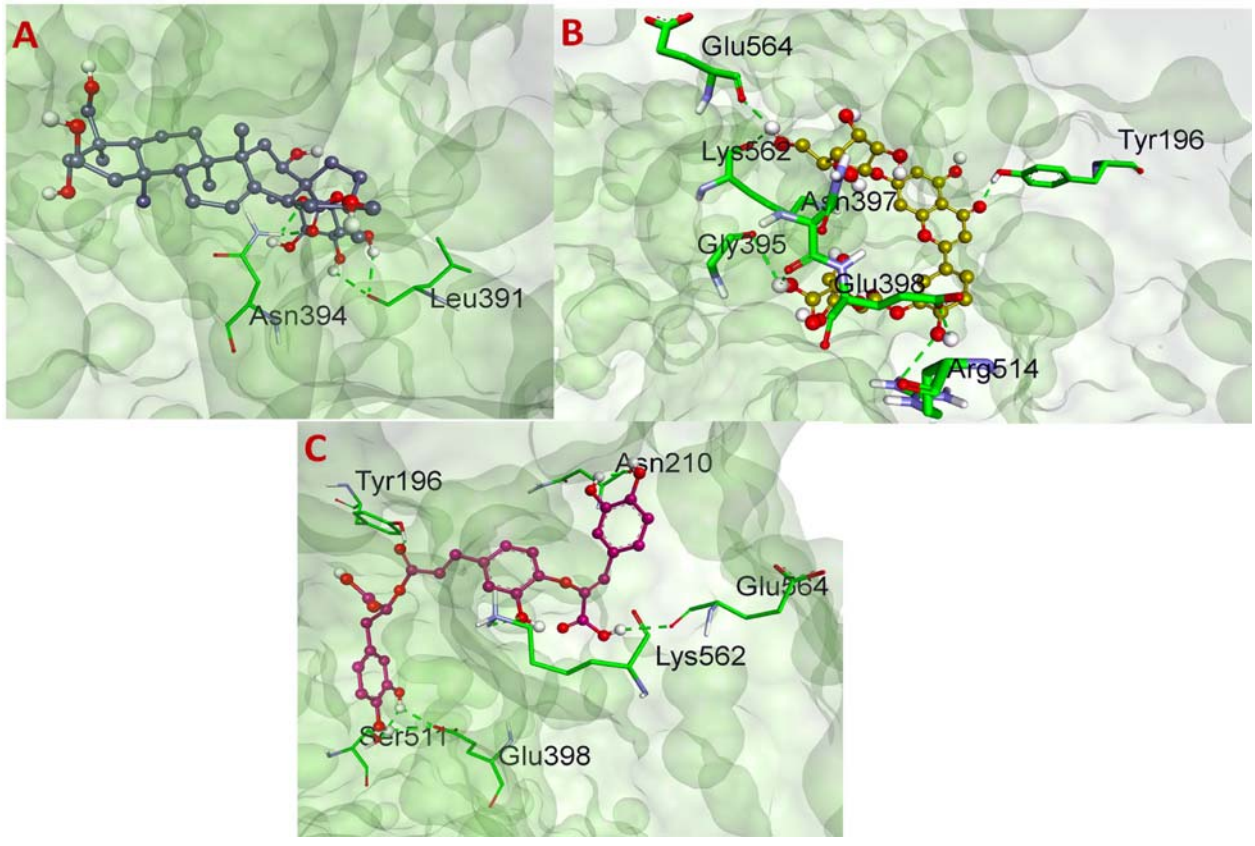

Figure 8. (Colour online) 3D Interactions of ligands with COVID-19 Spike Protein via Hydrogen Bonding. (A) Luteolin-7-glucoside-3′-glucuronide (B) Melitric acid A (C) Quadranoside III.

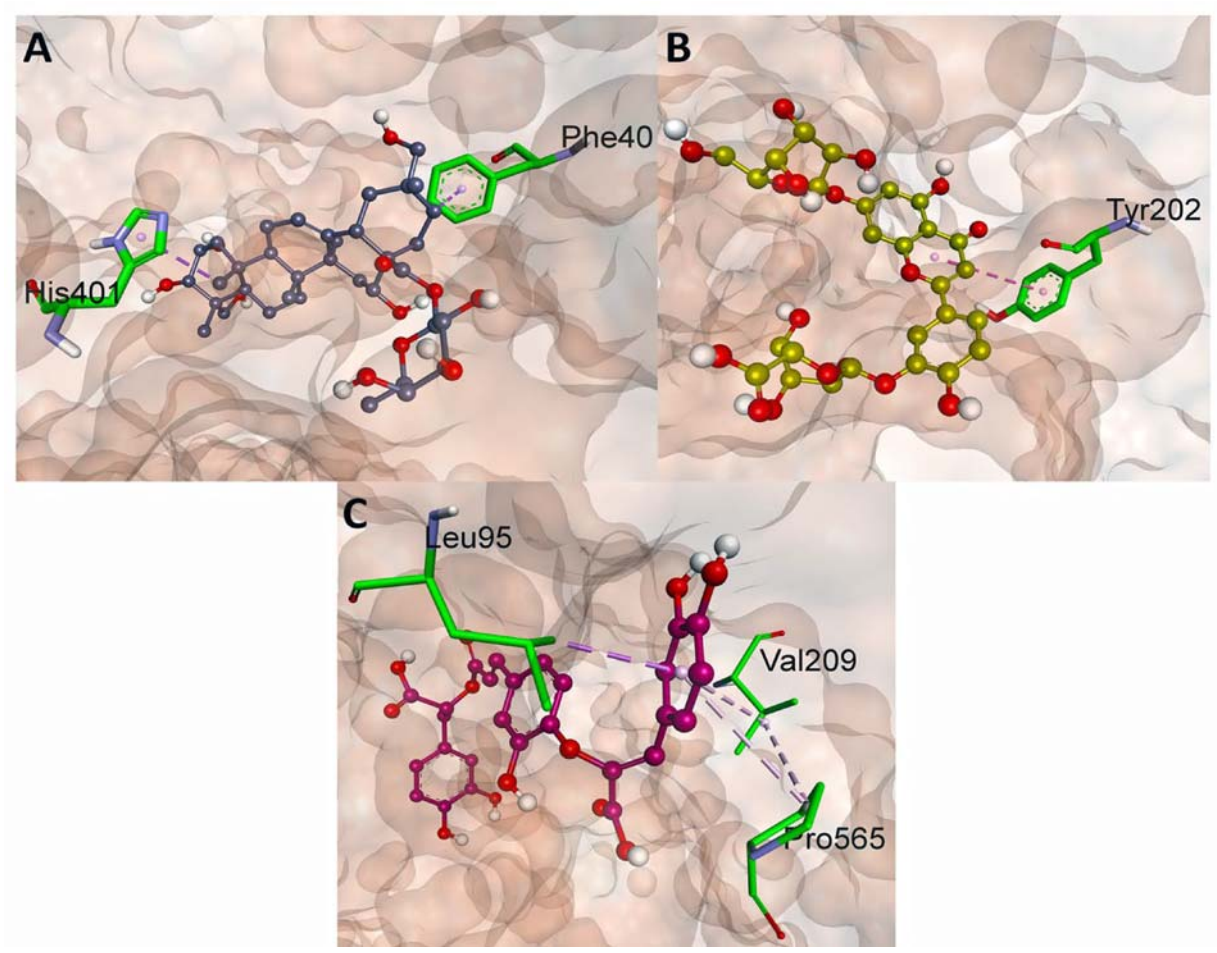

Figure 9. (Colour online) 3D Interactions of ligands with the COVID-19 Spike Protein via Hydrophobic Bonding. (A) Luteolin-7-glucoside-3′-glucuronide (B) Melitric acid A (C) Quadranoside III.

prevention, control and help. No specific clinical treatments for SARS-CoV-2-mediated infections are currently available [54]. It is, therefore, necessary to identify and discover potential drug candidates to overcome the loss of health caused by SARS-CoV-2.

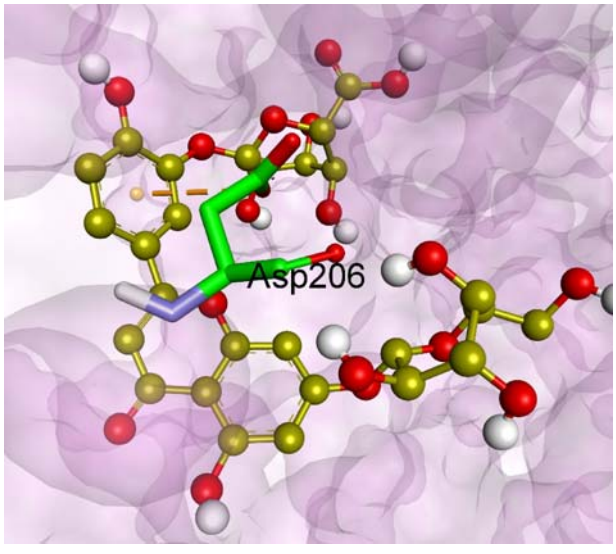

Figure 10. (Colour online) 3D Interactions of Melitric acid A with the Spike Protein (6LZG) of COVID-19 via Electrostatic Interaction.

This recent discovery of Mpro in COVID-19 provided an excellent opportunity to recognise possible candidates for coronavirus treatment. In this way, natural products in the last few years have gained prominence, as successful anti-viral agents [55,56]. Because of the urgent need for COVID-19 therapeutics and natural products facilities in medicines development, we have screened *M. officinalis* phytoconstituents. The current study may help in identification or optimisation of potential hit molecule for further experimental investigation.

Our examination majorly concentrated on exploring in silico potential of phytochemical valuable novel constituents from the herbal plant of *M. officinalis* against COVID-19. From the docking results, three selected phytoconstituents from *M. officinalis* were specifically chosen for further molecular dynamics and MM-PBSA studies.

Three compounds, out of 12 candidates, had a higher binding affinity with lower energy binding to the main protease and spike protein. Regarding the main protease, Quadranoside III has a minimum binding energy of −8.6 kcal/mol, which forms three hydrogen bonds with three amino acids have been identified, i.e. LYS A:137 (4.60), ASN A:238 (4.52), GLU A:288 (4.82) and one hydrophobic interaction LEU A:272 (4.46). The bond length for hydrogen bonds is <5 A°, meaning that

Table 3. Interactions of COVID-19 Main Protease (PDB ID:6LU7) amino acid residues with ligands at receptor sites.

Ligands	Binding affinity, ΔG (kcal/mol)	Amino acids involved and Distance (A°)	
		Hydrogen binding interactions	Hydrophobic interactions
Quadranoside III	−8.6	LYS A:137 (4.60), ASN A:238 (4.52), GLU A:288 (4.82)	LEU A:272 (4.46)
Luteolin-7-glucoside-3′-glucuronide	−8.5	PHE A:219 (5.16), ASN A:221 (3.75, 3.78, 4.67), ASP A:263 (3.50, 3.90)	LEU A:220 (4.22)
Melitric acid A	−8.2	GLN A:110 (4.80, 5.234), ASN A:151 (4.23), ILE A:249 (3.34)	VAL A:104 (7.12), ILE A:106 (5.62), PHE A:294 (4.40), PRO A:293 (4.44), ILE A:249 (4.77)

Table 4. Interactions of COVID-19 Spike Protein (PDB ID:6LZG) amino acid residues with ligands at receptor sites.

Ligands	Binding affinity, ΔG (kcal/mol)	Amino acids involved and Distance (A°)		
		Hydrogen binding interactions	Hydrophobic interactions	Electrostatic interactions
Luteolin-7-glucoside-3′-glucuronide	−10.1	TYR A:196 (6.05), GLU A:564 (5.23), LYS A:562 (4.36), GLY A:395 (4.95), ASN A:397 (2.98), ARG A:514 (5.03), GLU A:398 (4.76)	TYR A: 202 (6.27), GLY A:205 (5.85)	–
Melitric acid A	−10	TYR A:196 (6.76), LYS A:562 (4.27), ASN A:210 (3.14, 4.84), GLU A:564 (5.97), SER A:511 (3.69), GLU A:398 (4.77, 5.23)	LEU A:95 (5.34), VAL A:209 (4.10), PRO A:565 (4.29)	ASP A:206 (5.09)
Quadranoside III	−9.2	LEU A:391 (3.25, 5.17), ASN A:394 (3.73, 5.10)	PHE A:40 (4.71), HIS A:401 (4.42)	–

Table 5. ADME/T properties of *Melissa officinalis* compounds.

Ligands	HIA	BBB	AMES toxicity	Carcinogenicity	LD_{50} in rat (mol/kg)
Luteolin-7-glucoside-3′-glucuronide	0.8238	0.7845	Non-toxic	Non-carcinogenic	3.0164
Melitric acid A	0.6596	0.5113	Non-toxic	Non-carcinogenic	2.2699
Quadranoside III	0.6195	0.6553	Non-toxic	Non-carcinogenic	3.1226

Table 6. Summary of PASS measurements for the anti-viral activity of *Melissa officinalis* isolated phytoconstituents.

Main predicted activity by PASS online	Luteolin-7-glucoside-3′-glucuronide		Melitric acid A		Quadranoside III	
	Pa	Pi	Pa	Pi	Pa	Pi
Antiviral (Rhinovirus)	–	–	0.348	0.162	0.410	0.081
Antiviral (HIV)	0.140	0.078	0.299	0.008	0.126	0.101
Antiviral (Influenza)	0.773	0.003	0.262	0.120	0.802	0.003
Antiviral (Herpes)	0.486	0.011	0.244	0.135	0.724	0.003
Antiviral (Hepatitis B)	0..463	0.007	0.222	0.067	0.300	0.033
Antiviral (Trachoma)	0.090	0.055	–	–	–	–
Viral Entry Inhibitor	–	–	0.205	0.138	-	–

Note: PASS = Prediction of Activity Spectra for Substances; Pi = probable inactivity.

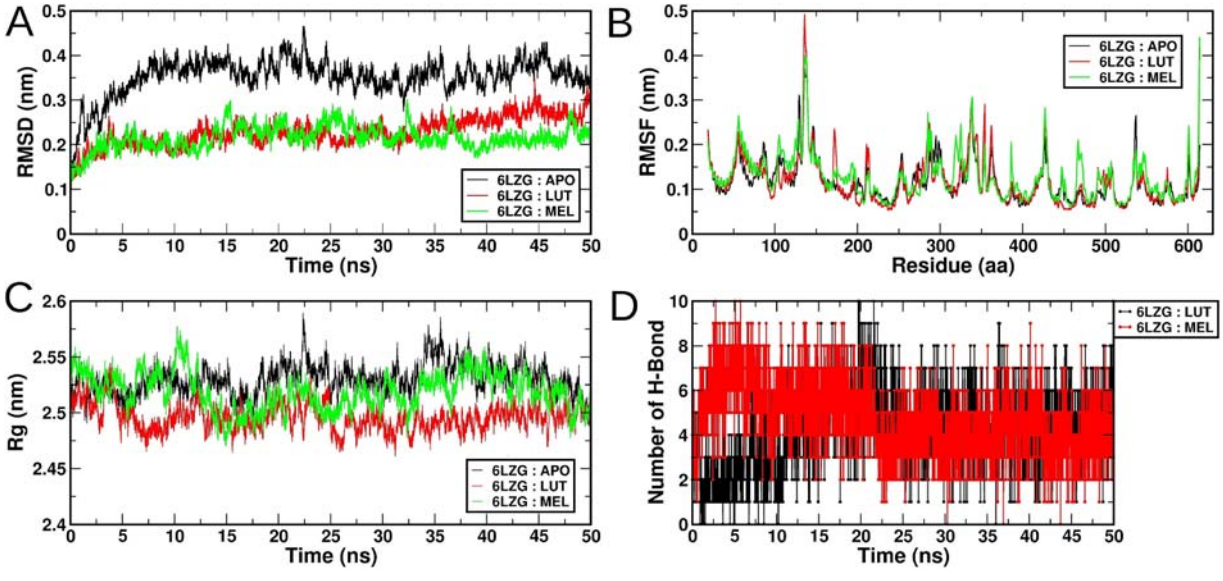

Figure 11. (Colour online) Simulation plots of active compounds with 6LZG A-RMSD plot; B-RMSF plot; C-Rg plot and D-Number of H-bonds over the simulation time.

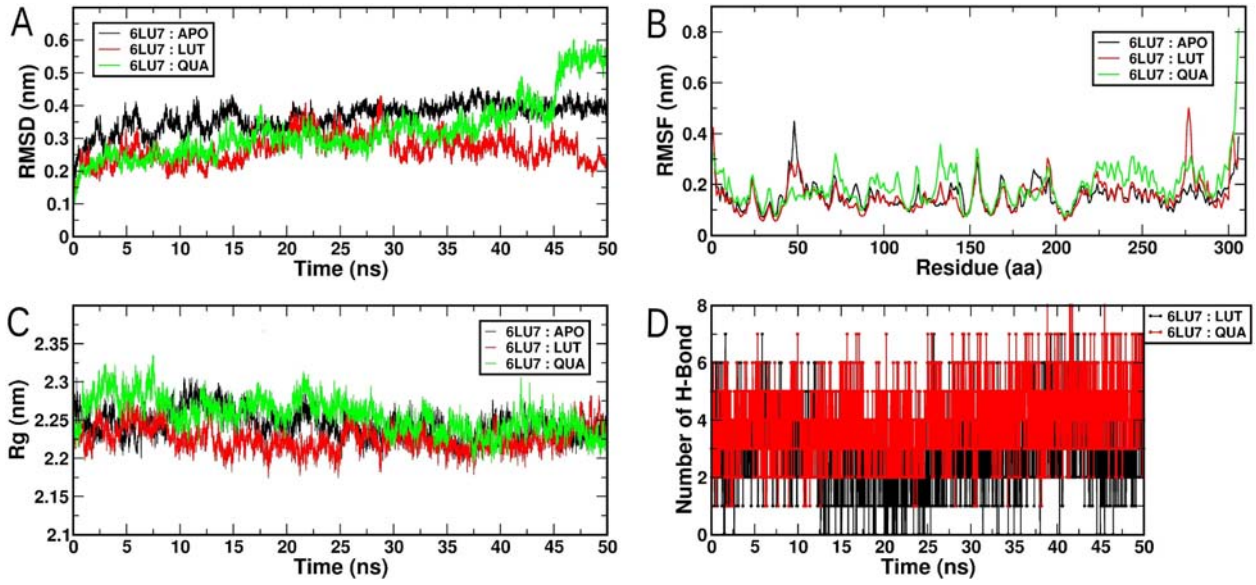

Figure 12. (Colour online) Simulation plots of active compounds with 6LU7 A-RMSD plot; B-RMSF plot; C-Rg plot and D-Number of H-bonds over the simulation time.

Table 7. Binding energy values and residue information of in silico potential complexes.

S. No	Complex	Binding energy (KJ/mol)	Active site residues within 6.5 A	Binding energy (KJ/mol)
1	6LU7-LUT	−84.035 ± 16.402	VAL-212, ILE-213, ARG-217, TRP-218, PHE-219, LEU-220, ASN-221, ARG-222, PHE-223, THR-257, ILE-259, ALA-266 SER-267, LEU-268, LYS-269, GLU-270, LEU-271, ASN-274, GLY-275, MET-276, ASN-277, ARG-279, VAL-303	−30.7317
2	6LU7-QUA	−82.056 ± 15.906	SER-139, ASN-203, VAL-204 TYR-237, TYR-239, LEU-268, GLU-270, LEU-271, LEU-272, GLN-273, ASN-274, GLY-275, MET-276, SER-284, ALA-285, LEU-286, LEU-287, GLU-288, ASP-289, GLU-290, PHE-291	−34.8114
3	6LZG-LUT	−106.398 ± 25.384	GLN-81, LEU-85, LEU-95, GLN-96, LEU-97, GLN-98, ALA-99, LEU-100, GLN-101, GLN-102, ASN-103, GLY-104, SER-105, LYS-187, MET-190, ASN-194, HIS-195, TYR-196, TYR-199, ASP-201, TYR-202, TRP-203, ARG-204, GLY-205, ASP-206, TYR-207, GLU-208, VAL-209, ASN-210, ALA-396, ARG-460, ASP-509, TYR-510, SER-511, ILE-513, LYS-562, PRO-565, TRP-566	−6.5807
4	6LZG-MEL	−137.222 ± 18.027	LEU-91, LEU-95, GLN-98, ALA-99, GLN-102, ASN-103, GLY-104, TYR-196, TYR-202, TRP-203, ARG-204, GLY-205, ASP-206, TYR-207, GLU-208, VAL-209, ASN-210, GLY-211, VAL-212, ARG-219, GLY-395, ALA-396, ASN-397, GLU-398, ASP-509, ARG-514, GLY-561, LYS-562, SER-563, GLU-564, PRO-565, TRP-566, THR-567.	−7.2158

the bond is stronger and stable complexes are produced. Although luteolin-7-glucoside-3′-glucuronide has a binding energy of −8.5 kcal/mol, it was associated with three hydrogen bonds with PHE A:219 (5.16), ASN A:221 (3.75, 3.78, 4.67), ASP A:263 (3.50, 3.90) and hydrophobic interactions with LEU A:220 (4.22). Melitric acid A established hydrogen bonding with GLN A:110 (4.80, 5.234), ASN A:151 (4.23), ILE A:249 (3.34) and hydrophobic interactions with VAL A:104 (7.12), ILE A:106 (5.62), PHE A:294 (4.40), PRO A:293 (4.44), ILE A:249 (4.77). In comparison with other ligands, these three compounds were least binding due to the formation of more hydrogen bonds with the proteins. Surprisingly, out of all three compounds, no one involved in electrostatic interactions.

Concerning Spike protein, Luteolin-7-glucoside-3′-glucuronide demonstrated the least binding energy of −10.1 kcal/mol and found to make seven hydrogen bonds with three amino acids, i.e. TYR A:196 (6.05), GLU A:564 (5.23), LYS A:562 (4.36), GLY A:395 (4.95), ASN A:397 (2.98), ARG A:514 (5.03), GLU A:398 (4.76). Also formed two hydrophobic interactions with TYR A: 202 (6.27), GLY A:205 (5.85). Melitric acid A formed hydrogen bonding with TYR A:196 (6.76), LYS A:562 (4.27), ASN A:210 (3.14, 4.84), GLU A:564 (5.97), SER A:511 (3.69), GLU A:398 (4.77, 5.23); hydrophobic interactions with LEU A:95 (5.34), VAL A:209 (4.10), PRO A:565 (4.29) and electrostatic interaction with ASP A:206 (5.09). Quadranoside III established hydrogen bonding with LEU A:391 (3.25, 5.17), ASN A:394 (3.73, 5.10) and hydrophobic interactions with PHE A:40 (4.71), HIS A:401 (4.42).

Our previous study identified tenufolin and Pavetannin C1 from Cinnamon with good binding affinity and stability against same Mpro and Spike protein from docking, molecular dynamics and MM-PBSA calculations. Mpro-tenufolin complex was stabilised with binding energy value of −123.949 ± 16.613 kJ/mol and spike protein-Pavetannin C1 complex with −158.870 ± 30.378 kJ/mol, respectively [34]. In comparison with binding energy values in Table 7, *M. officinalis* compounds have exhibited higher binding energy values in GROMACS MM-PBSA calculations. Further experimental investigation will give a better understanding about the efficacy of compounds isolated from Cinnamon or *M. officinalis*.

Interesting correlation was observed with the docking results and molecular weight of compounds taken in the study. However, a number of compounds taken were very

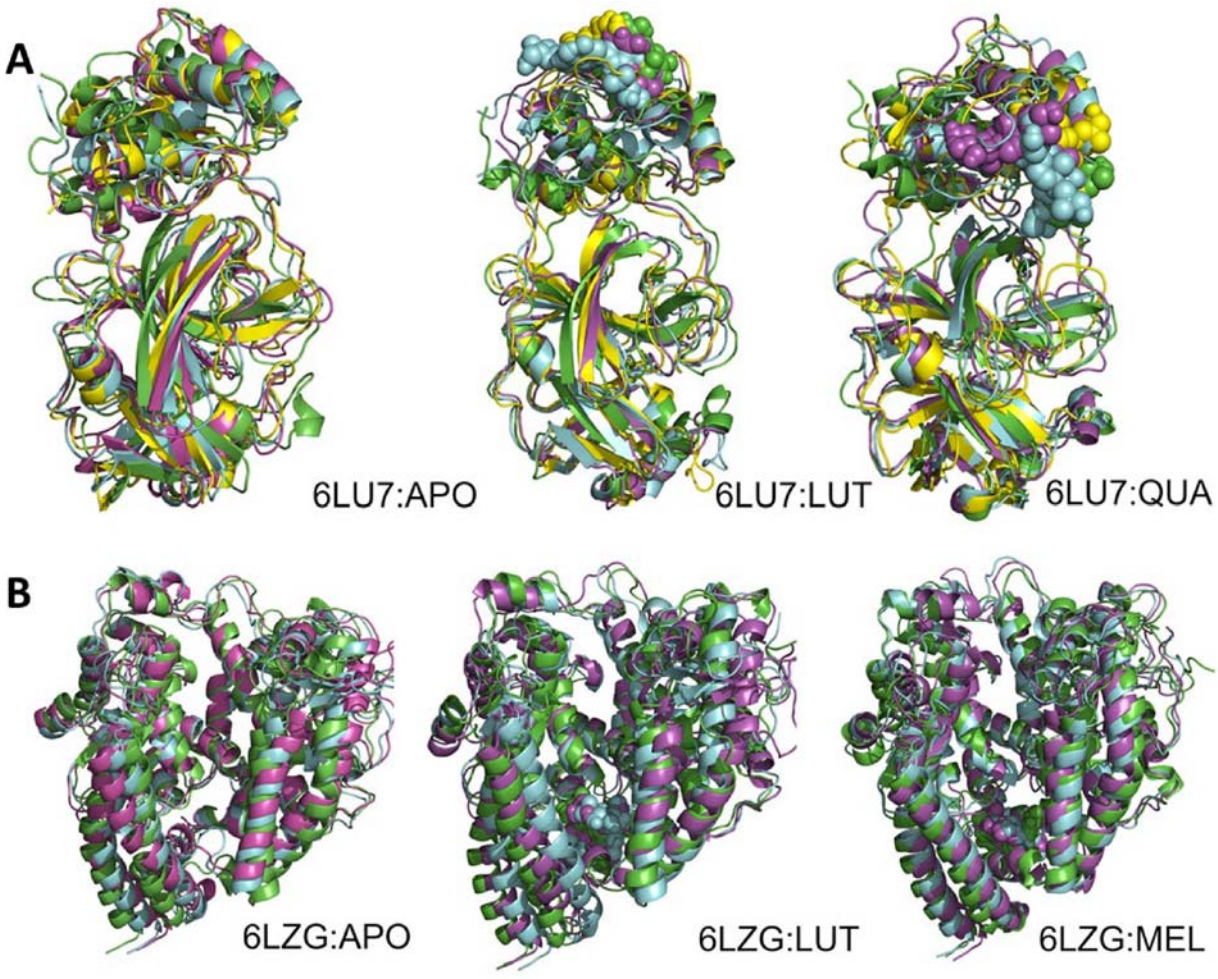

Figure 13. (Colour online) (A) Time scale analysis of 6LU7 systems in dynamics 0 ns (green colour), 100 ns (cyan colour), 200 ns (magenta colour) and 300 ns (yellow colour), (B) Time scale analysis of 6LZG systems in dynamics 0 ns (green colour), 50 ns (cyan colour), 100 ns (magenta colour).

few and does not have a wide range of molecular weight. Three compounds Quadranoside III, Luteolin-7-glucoside-3′-glucuronide and Melitric acid A have a molecular weight of 666.846, 625.51 and 538.46 g/mol, respectively. All three compounds have demonstrated good binding affinity and stability in molecular dynamics integrated with MM-PBSA calculations against both target proteins. The next two compounds were Labiatenic acid and Nepetoidin A with a molecular weight of 360.317 and 314.292 g/mol have exhibited less binding affinity in comparison with the above three compounds. All the other compounds have a molecular weight of less than 200 g/mol and also observed poor docking results. The study indicates that the active pocket of both target proteins has the ability to accommodate large molecules. However, validation with experimental results will give a clear understanding of the relation with molecular weight of compounds.

Lipinski's five-rule is a primary standard for assessing drug likeliness. Lipinski's law specifies the molecular properties essential to the pharmacokinetics of medication in the human body, such as ADME. Lipinski's rule of five conditions for optimal medicines. The top three scored compounds failed to obey Lipinski's rule, specifically in the number of H-bond donors and acceptors, as they were derived from natural origin. ADME predictions of selected three compounds have qualified the ADME check screens (Table 3). From the MD simulations and MM-PBSA calculations, 6LU7-LUT and 6LZG-MEL complexes were found stable and recognised as potential *in silico* inhibitors for respective target proteins. This preliminary screening of possible molecules (anti-virals) will help to provide rapid input for further experimental analysis against SARS-CoV-2 (COVID-19).

5. Conclusion

In the research, we used bioinformatics tools, Autodock, GROMACS, admetSAR and PASS analysis to recognise the potential *Manosa officinalis* molecules against COVID-19 main proteases and spike target proteins. Our findings suggest that the two phytoconstituents, Luteolin-7-glucoside-3′-glucuronide and Melitric acid-A, should be extended for *in vitro* and pre-clinical studies as potential inhibitors to COVID-19 main proteases and spike-proteins.

Disclosure statement

No potential conflict of interest was reported by the authors.

ORCID

D. S. N. B. K. Prasanth http://orcid.org/0000-0001-5028-1283
Murahari Manikanta http://orcid.org/0000-0002-5404-4426

References

[1] World Health Organization. Coronavirus disease 2019 (COVID-19): situation report, 70. 2020.
[2] Chen N, Zhou M, Dong X, et al. Epidemiological and clinical characteristics of 99 cases of 2019 novel coronavirus pneumonia in Wuhan, China: a descriptive study. Lancet. 2020;395:507–513.
[3] Rouchka EC, Chariker JH, Chung D. Phylogenetic and variant analysis of 1,040 SARS-CoV-2 Genomes. 2020.
[4] Lu R, Zhao X, Li J, et al. Genomic characterisation and epidemiology of 2019 novel coronavirus: implications for virus origins and receptor binding. Lancet. 2020;395:565–574.
[5] Jin Z, Du X, Xu Y, et al. Structure of Mpro from COVID-19 virus and discovery of its inhibitors. bioRxiv. Preprint. 2020.
[6] Hui DS, Azhar EI, Madani TA, et al. The continuing 2019-nCoV epidemic threat of novel coronaviruses to global health – The latest 2019 novel coronavirus outbreak in Wuhan, China. Int J Infect Dis. 2020;91:264–266.
[7] Moses T, Goossens A. Plants for human health: greening biotechnology and synthetic biology. J Exp Bot. 2017;68:4009–4011.
[8] Schaal B. Plants and people: our shared history and future. Plants People Planet. 2019;1:14–19.
[9] Jassim SAA, Naji MA. Novel antiviral agents: a medicinal plant perspective. J Appl Microbiol. 2003;95:412–427.
[10] Hussain W, Haleem KS, Khan I, et al. Medicinal plants: a repository of antiviral metabolites. Future Virol. 2017;12:299–308.
[11] Özçelik B, Kartal M, Orhan I. Cytotoxicity, antiviral and antimicrobial activities of alkaloids, flavonoids, and phenolic acids. Pharm Biol. 2011;49:396–402.
[12] Ling APK, Khoo B, Seah C, et al. Inhibitory activities of methanol extracts of Andrographis paniculata and Ocimum sanctum against dengue-1 virus. 2014: Publisher.
[13] Murgueitio MS, Bermudez M, Mortier J, et al. In silico virtual screening approaches for anti-viral drug discovery. Drug Discov Today: Technol. 2012;9:e219–e225.
[14] Castro T, Barbosa K, Albarello N, et al. Caracterização de pseudofrutos, frutos, sementes e plântulas obtidas a partir de germinação in vivo e in vitro da espécie medicinal Hovenia dulcis (Rhamnaceae). Revista Cubana de Plantas Medicinales. 2005;10:1–16.
[15] Shen B. A new golden age of natural products drug discovery. Cell. 2015;163:1297–1300.
[16] Thomford N, Senthebane D, Rowe A, et al. Natural products for drug discovery in the 21st century: innovations for novel drug discovery. Int J Mol Sci. 2018;19:1578.
[17] Rastogi S, Pandey DN, Singh RH. COVID-19 pandemic: a pragmatic plan for ayurveda intervention. J Ayurveda Integr Med. 2020. DOI:10.1016/j.jaim.2020.04.002
[18] Panyod S, Ho C-T, Sheen L-Y. Dietary therapy and herbal medicine for COVID-19 prevention: a review and perspective. J Tradit Complement Med. 2020;10:420–427.
[19] Cao P, Wu S, Wu T, et al. The important role of polysaccharides from a traditional Chinese medicine-lung cleansing and detoxifying decoction against the COVID-19 pandemic. Carbohydr Polym. 2020;240:116346.
[20] Mimica-Dukic N, Bozin B, Sokovic M, et al. Antimicrobial and antioxidant activities of *Melissa officinalis* L. (Lamiaceae) essential oil. J Agric Food Chem. 2004;52:2485–2489.
[21] Schnitzler P, Schuhmacher A, Astani A, et al. Melissa officinalis oil affects infectivity of enveloped herpesviruses. Phytomedicine. 2008;15:734–740.
[22] Allahverdiyev A, Duran N, Ozguven M, et al. Antiviral activity of the volatile oils of *Melissa officinalis* L. against Herpes simplex virus type-2. Phytomedicine. 2004;11:657–661.
[23] Akhondzadeh S, Noroozian M, Mohammadi M, et al. *Melissa officinalis* extract in the treatment of patients with mild to moderate Alzheimer's disease: a double blind, randomised, placebo controlled trial. J Neurol Neurosurg Psychiatry. 2003;74:863–866.
[24] López V, Martin S, Gómez-Serranillos MP, et al. Neuroprotective and neurological properties of *Melissa officinalis*. Neurochem Res. 2009;34:1955–1961.
[25] Encalada MA, Hoyos KM, Rehecho S, et al. Anti-proliferative effect of *Melissa officinalis* on human colon cancer cell line. Plant Foods Hum Nutr. 2011;66:328–334.
[26] Čanadanović-Brunet J, Ćetković G, Djilas S, et al. Radical scavenging, antibacterial, and antiproliferative activities of *Melissa officinalis* L. extracts. J Med Food. 2008;11:133–143.
[27] Bolkent S, Yanardag R, Karabulut-Bulan O, et al. Protective role of *Melissa officinalis* L. extract on liver of hyperlipidemic rats: a morphological and biochemical study. J Ethnopharmacol. 2005;99:391–398.
[28] Emamghoreishi M, Talebianpour M. Antidepressant effect of *Melissa officinalis* in the forced swimming test. DARU J Pharm Sci. 2015;17:42–47.
[29] Chung MJ, Cho S-Y, Bhuiyan MJ, et al. Anti-diabetic effects of lemon balm (*Melissa officinalis*) essential oil on glucose- and lipid-regulating enzymes in type 2 diabetic mice. Br J Nutr. 2010;104:180–188.
[30] Mohanraj K, Karthikeyan BS, Vivek-Ananth RP, et al. IMPPAT: a curated database of Indian MEdicinal PLants, Phytochemistry And Therapeutics. Sci Rep. 2018;8:1–17.
[31] Chaudhuri S, Symons JA, Deval J. Innovation and trends in the development and approval of antiviral medicines: 1987–2017 and beyond. Antiviral Res. 2018;155:76–88.
[32] Sander T, Freyss J, von Korff M, et al. Datawarrior: an open-source program for chemistry aware data visualization and analysis. J Chem Inf Model. 2015;55:460–473.
[33] Sussman JL, Lin D, Jiang J, et al. Protein Data Bank (PDB): database of three-dimensional structural information of biological macromolecules. Acta Crystallogr D Biol Crystallogr. 1998;54:1078–1084.
[34] Prasanth DSNBK, Murahari M, Chandramohan V, et al. *In silico* identification of potential inhibitors from *Cinnamon* against main protease and spike glycoprotein of SARS CoV-2. J Biomol Struct Dyn. 2020:1–15. DOI:10.1080/07391102.2020.1779129
[35] Kar P, Sharma NR, Singh B, et al. Natural compounds from Clerodendrum spp. as possible therapeutic candidates against SARS-CoV-2: An in silico investigation. J Biomol Struct Dyn. 2020:1–12. DOI:10.1080/07391102.2020.1780947
[36] Morris GM, Huey R, Lindstrom W, et al. Autodock4 and AutoDockTools4: Automated docking with selective receptor flexibility. J Comput Chem. 2009;30:2785–2791.
[37] O'Boyle NM, Banck M, James CA, et al. Open Babel: an open chemical toolbox. J Cheminform. 2011;3:33.
[38] Pangastuti A, Amin IF, Amin AZ, et al. Natural bioactive compound from Moringa oleiferaagainst cancer based on in silico screening. Jurnal Teknologi. 2016;78:315–318.
[39] Dallakyan S, Olson AJ. Small-molecule library screening by docking with PyRx. 2015;1263:243–250.
[40] Seeliger D, de Groot BL. Ligand docking and binding site analysis with PyMOL and Autodock/Vina. J. Comput. Aided Mol. Des.. 2010;24:417–422.
[41] Yang H, Lou C, Sun L, et al. admetSAR 2.0: web-service for prediction and optimization of chemical ADMET properties. Bioinformatics. 2019;35:1067–1069.
[42] Cheng F, Li W, Zhou Y, et al. admetSAR: a comprehensive source and free tool for assessment of chemical ADMET properties. J Chem Inf Model. 2012;52:3099–3105.
[43] Khurana N, Ishar MPS, Gajbhiye A, et al. PASS assisted prediction and pharmacological evaluation of novel nicotinic analogs for nootropic activity in mice. Eur J Pharmacol. 2011;662:22–30.
[44] Mittal M, Goel RK, Bhargava G, et al. PASS-assisted exploration of antidepressant activity of 1,3,4-trisubstituted-β-lactam derivatives. Bioorg Med Chem Lett. 2008;18:5347–5349.

[45] Goel RK, Singh D, Lagunin A, et al. PASS-assisted exploration of new therapeutic potential of natural products. Med Chem Res. 2011;20:1509–1514.
[46] Van Der Spoel D, Lindahl E, Hess B, et al. GROMACS: fast, flexible, and free. J Comput Chem. 2005;26:1701–1718.
[47] Gangadharappa BS, Sharath R, Revanasiddappa PD, et al. Structural insights of metallo-beta-lactamase revealed an effective way of inhibition of enzyme by natural inhibitors. J Biomol Struct Dyn. 2020;38:3757–3771.
[48] Chandramohan V, Kaphle A, Chekuri M, et al. Evaluating andrographolide as a potent inhibitor of NS3-4A protease and its drug-resistant mutants using *in silico* approaches. Adv Virol. 2015;2015:972067.
[49] Schüttelkopf AW, van Aalten DMF. *PRODRG*: a tool for high-throughput crystallography of protein-ligand complexes. Acta Crystallogr D Biol Crystallogr. 2004;60:1355–1363.
[50] Gulans A, Kontur S, Meisenbichler C, et al. Exciting: a full-potential all-electron package implementing density-functional theory and many-body perturbation theory. J Phys Condens Matter. 2014;26:363202.
[51] Ertl P, Rohde B, Selzer P. Fast calculation of molecular polar surface area as a sum of fragment-based contributions and its application to the prediction of drug transport properties. J Med Chem. 2000;43:3714–3717.
[52] To KK, Hung IF, Chan JF, et al. From SARS coronavirus to novel animal and human coronaviruses. J Thorac Dis. 2013;5(Suppl 2):S103–S108.
[53] Zhu N, Zhang D, Wang W, et al. A novel coronavirus from patients with pneumonia in China, 2019. N Engl J Med. 2020;382:727–733.
[54] Zhou Y, Hou Y, Shen J, et al. Network-based drug repurposing for novel coronavirus 2019-nCoV/SARS-CoV-2. Cell Discov. 2020;6:14.
[55] Lin L-T, Hsu W-C, Lin C-C. Antiviral natural products and herbal medicines. J Tradit Complement Med. 2014;4:24–35.
[56] Martinez JP, Sasse F, Brönstrup M, et al. Antiviral drug discovery: broad-spectrum drugs from nature. Nat Prod Rep. 2015;32:29–48.